Alignment, Mining and Fusion: Representation Alignment with Hard Negative Mining and Selective Knowledge Fusion for Medical Visual Question Answering

Yuanhao Zou University of Michigan, Ann Arbor

yuanhaoz@umich.edu

Zhaozheng Yin* Stony Brook University

zyin@cs.stonybrook.edu

Abstract

Medical Visual Question Answering (Med-VQA) is a challenging task that requires a deep understanding of both medical images and textual questions. Although recent works leveraging Medical Vision-Language Pre-training (Med-VLP) have shown strong performance on the Med-VQA task, there is still no unified solution for modality alignment, and the issue of hard negatives remains underexplored. Additionally, commonly used knowledge fusion techniques for Med-VQA may introduce irrelevant information. In this work, we propose a framework to address these challenges through three key contributions: (1) a unified solution for heterogeneous modality alignments across multiple levels, modalities, views, and stages, leveraging methods like contrastive learning and optimal transport theory; (2) a hard negative mining method that employs soft labels for multi-modality alignments and enforces the hard negative pair discrimination; and (3) a Gated Cross-Attention Module for Med-VQA that integrates the answer vocabulary as prior knowledge and selects relevant information from it. Our framework outperforms the previous state-ofthe-art on widely used Med-VQA datasets like RAD-VQA, SLAKE, PathVQA and VQA-2019. The code is available at https://github.com/AlexCold/AMiF

1. Introduction

Medical Visual Question Answering (**Med-VQA**) is a task that requires a joint understanding of both medical texts and images, aiding in clinical decision-making [34]. While deep learning models have made significant strides in general visual question answering tasks [39], Med-VQA presents unique challenges, such as the presence of obscure objects in images and relatively smaller scale of annotated medical datasets for training models [16, 50]. To address these challenges, many existing works [9, 10, 15, 22, 29, 30, 52] utilize Vision-Language Pre-training (**VLP**), achieving re-

markable success in the medical domain (*i.e.*, Medical Vision-Language Pre-training, **Med-VLP**). These methods employ self-supervised learning to pre-train models on large unannotated medical datasets (*e.g.*, MIMIC-CXR [24]), initializing their models with the ability to extract medical visual-language representations. The models are then fine-tuned for downstream tasks like Med-VQA.

Among Med-VLP research, self-supervised techniques such as Contrastive Learning [6, 46, 58] are widely used to train visual and textual encoders to align representations between images and texts. While some works [5, 15, 29, 30, 54, 57–59] perform the global-level alignment (i.e., align only the [CLS] token of images and texts), other works [12, 22, 40, 52] attempt the local-level alignment, matching the similarity between image tokens and text tokens. However, these works focus on the inter-modality information (aligning images with texts), ignoring that medical datasets for Med-VLP (e.g., MIMIC-CXR [24]) contain valuable intra-modality similarities within images and reports. Though works like MUMC [29] attempt to align features within uni-modality, they do not perform local-level alignment and overlook the multi-view attribute of radiology imaging, which can naturally be used for intra-modality alignment. A unified approach that simultaneously addresses global-level alignment for both inter-modality (image-text) and intra-modality (image-image & text-text), and local-level alignment remains under-explored.

Additionally, contrastive learning methods like CLIP [46] treat image-text *pairs* (image-text from the same patient) as positive samples, with unpaired images and texts as negative samples. However, in the medical domain, because of similar clinical manifestations of the same diseases, consistent anatomical imaging patterns, and standardized reporting practices, high similarities exist between unpaired images and texts, resulting in numerous hard negatives. While most of the prior CLIP-based works [5, 15, 22, 30, 52, 57–59] employ one-hot labels for contrastive learning, they overlook the issue of hard negatives in the medical domain. Though prior works [7, 29, 33, 54] use soft labels for hard negatives, their methods primarily

^{*}Corresponding author

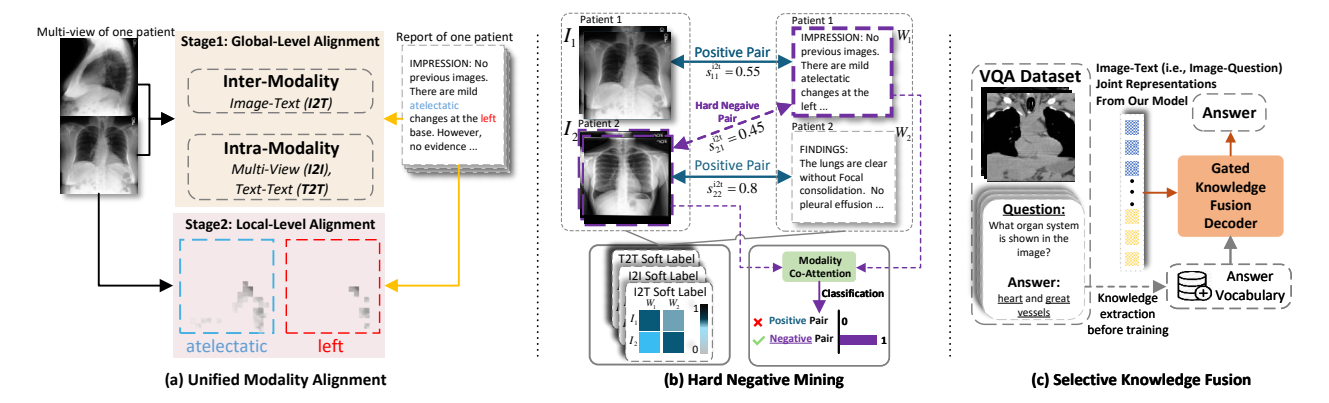


Figure 1. Motivations on: (a) unified modality alignment, (b) hard negative mining, and (c) selective knowledge fusion for Med-VQA.

consider hard negatives derived from image-text similarity (*i.e.*, inter-modality), neglecting that the tight relationships within images and reports (*i.e.*, intra-modality) could also be leveraged to explore hard negatives. Moreover, these soft label approaches calculate non-zero or even high similarity scores for hard negative pairs, making it hard to explicitly distinguish them from positive pairs. Thus, *hard negative mining*, *i.e.*, distinguishing hard negative pairs from positive pairs for both inter-modality and intra-modality could be significantly improved in the medical domain.

For fine-tuning downstream tasks like Med-VQA, fusing prior knowledge with the input image-question representation is a common practice to enhance the model's question-answering capability [10, 13, 16, 36, 41, 44, 53]. For example, many methods introduce knowledge graph matrices from Unified Medical Language System (UMLS, [3]) as prior knowledge. This prior knowledge contains terminology that covers a comprehensive scope of the medical domain, while a downstream task may only focus on a specific medical imaging modality or a specific human organ. Therefore, fusing untrimmed knowledge may introduce irrelevant or unnecessary information. For Med-VQA, a method that can selectively fuse appropriate prior knowledge with the joint image-question representation will lead to a better question-answering ability for the model.

In this paper, to unify heterogeneous modality alignments and address the challenges of hard negatives and knowledge fusion in Medical Visual Question Answering, we propose a systematic framework named AMiF: Representation Alignment with Hard Negative Mining and Selective Knowledge Fusion. Our detailed contributions are:

We unify various modality alignments (Fig. 1 (a)) for medical representation learning at Multi-level: we use contrastive learning method for global-level alignment and optimal transport theory for local-level alignment; Multi-modality: we align not only the inter-modality (I2T: image-text) but also the intra-modality (I2I: image-image, T2T: text-text); Multi-view: we leverage the

unique multi-view attribute in the medical datasets for the intra-modality I2I alignment; and **Multi-stage**: we focus on the global-level alignment in the first stage of pre-training, and then focus on local-level alignment and hard negative mining in the second stage.

- We propose a hard negative mining method (Fig. 1
 (b)) that operates across multiple modalities during pretraining. Specifically, for both inter-modality and intramodality alignments, we employ soft labels that assign non-zero values to negative pairs, which reflect the nuanced similarities between their representations due to similar disease characteristics. Subsequently, hard negative pairs mistakenly with high similarities are enforced to be identified and differentiated from positive pairs, helping AMiF learn discriminative image-text joint feature representations.
- For the Med-VQA task (Fig. 1 (c)), we extract the answer vocabulary from the task-specific dataset as prior knowledge. We introduce a Gated Cross-Attention Module to fuse the prior knowledge into the image-text joint representation. Then, the gated operation in the module selects useful information from the knowledge-fused representation to enhance model performance on VQA tasks.
- By applying the above techniques, our proposed AMiF shows its effectiveness on the Med-VQA tasks, evaluated on widely-used benchmark datasets including RAD-VQA [27], SLAKE [36], PathVQA [18] and VQA-2019 [2].

2. Related Works

2.1. Modality Alignment for Med-VLP

While global-level alignment [5, 15, 29, 30, 54, 57–59] aligns the high-level [CLS] token of the modality representations, local-level alignment attempts to match all tokens of the representations. Numerous works have investigated the local-level alignment in the medical domain. Notably, Liao *et al.* compute the mutual information between local tokens [31], while GLoRIA [22], LRCLR [47], LoVT

[40] and LIMITR [12] explore using contrastive learning to align image patch tokens and report tokens at local-level [48]. MGCA [52] uses a cross-attention module for local alignment. Unlike the idea of contrastive learning, UNITER [8] and ViLT [26] apply the Optimal Transport (OT) theory and IPOT algorithm [55] to optimize a transport plan for local-level alignment in the natural domain. The OT theory has not been used for Med-VLP yet. For multi-modality alignment, MUMC [29] introduces uni-modality alignment within images or texts. While LIMITR [12] compares both the frontal view and lateral view with the text representations. Our approach, which also explores multi-view images, focuses on alignment within the multi-view representations and unifies heterogeneous local-level alignment and global-level alignment on both inter- and intra-modalities.

2.2. Hard Negatives for Med-VLP

For Med-VLP, CLIP-based methods use the one-hot label for image-text pairs [5, 15, 29, 30, 54, 57-59], ignoring the hard negatives caused by the similarity between unpaired image-text representations in the medical domain. Many efforts attempt to solve the hard negative problem by applying soft label supervision for contrastive learning [1, 14, 20, 28, 35, 45]. In the medical domain, Jang et al. relax the similarity function by clipping the upper bound [23], ReCO [33] applies less penalty for the negative pairs, while MedCLIP [54] and KoBo [7] use soft label from external knowledge. In addition, MUMC [29] uses the selfdistillation technique [28] to learn from the soft label generated itself. Different from the above studies, our approach explores hard negative mining in the medical domain. We not only use soft labels for hard-negative pairs of both intermodality and intra-modality alignments but also attempt to further distinguish the hard negatives from the positives.

2.3. Med-VQA and Knowledge Fusion

For Med-VQA, prior works like MEVF [41] and MMQ [13] attempt to train a meta-model using additional data besides the Med-VQA dataset to facilitate VQA performance. Other methods [9, 10, 15, 29, 30, 57] employ Med-VLP to initialize the model weight on large unlabeled datasets via self-supervised learning. Besides, without pre-training, other approaches introduce structured prior knowledge. For instance, LaPA [16] utilizes a knowledge graph [51] with well-stored medical information as its prior knowledge, integrating auxiliary information for more relevant answer prediction. Our approach uses answer vocabulary from the specific Med-VQA datasets as prior knowledge and enables selective knowledge fusion via a Gated Cross-Attention Module. Moreover, most prior works [9, 10, 16, 30] treat Med-VQA as a multi-labels classification task, using a fixed number of answers for prediction, while our model generates *open*-form answers like [28, 38].

3. Methodology

3.1. Overview

As illustrated in Fig. 2, we divide the training process of AMiF into two phases: (a) pre-training and (b) fine-tuning.

In pre-training phase, we use the medical pre-training dataset $\{(I_i,W_i)\}_{i=1}^N$, where N is the dataset sample number and $I_i=\{I_i^{(1)},\ldots,I_i^{(v_i)}\}$ is one imaging study case corresponding to one patient. We randomly sample multiple views from I_i , which corresponds to a single report W_i . If the case I_i does not have multiple views (i.e., $v_i=1$), we augment the identical view multiple times. These multiview images are then encoded by a visual encoder, resulting in multi-view representations $V_i^{(1)}, V_i^{(2)}$ (the number of multi-view is chosen as 2 in this paper), while the corresponding report is encoded as report representation R_i . We split the pre-training into two stages: (1) Global-Level Alignment with soft labels, and (2) Tokens are further matched between V_i and R_i , where V_i is a random selection between $V_i^{(1)}$ and $V_i^{(2)}$.

In the fine-tuning phase, our AMiF utilizes the initialized weights (*i.e.*, visual encoder, textual encoder, and Modality Co-Attention Module) from the pre-training phase, and is then adapted to the Med-VQA task via a Gated Knowledge Fusion Decoder, which takes answer vocabulary from the specific Med-VQA dataset as the prior knowledge and generates answers via an auto-regressive decoder.

3.2. Unified Modality Alignment

3.2.1 Global-Level Alignment

Given the multi-view representations $V_i^{(1)}, V_i^{(2)}$ and text representation R_i extracted by the visual and textual encoders, their <code>[CLS]</code> tokens are denoted as $\boldsymbol{v}_i^{(1)}, \boldsymbol{v}_i^{(2)}, \boldsymbol{r}_i \in \mathbb{R}^d$ respectively (d is the token embedding dimension), which are used for the following inter-modality alignment (image-text) and intra-modality alignment (split as multi-view alignment and text-text alignment).

Inter-Modality (Image-Text) First, we project the image and text embeddings v_i and r_i via a projection function $\operatorname{proj}(\cdot)$, where $v_i \in \{v_i^{(1)}, v_i^{(2)}\}$. Then, we compute the cosine similarity between the i-th image sample and the j-th text sample as:

$$s_{ij}^{\text{i2t}} = \text{proj}(\boldsymbol{v}_i)^{\top} \text{proj}(\boldsymbol{r}_j).$$
 (1)

The probability of aligning (or matching) image i with text report j is computed as:

$$P_{ij}^{\text{i2t}} = \frac{\exp(s_{ij}^{\text{i2t}}/\tau_1)}{\sum_{k=1}^{N} \exp(s_{ik}^{\text{i2t}}/\tau_1)},$$
 (2)

where τ_1 is a temperature parameter. The similar computation is applied to P_{ij}^{t2i} .

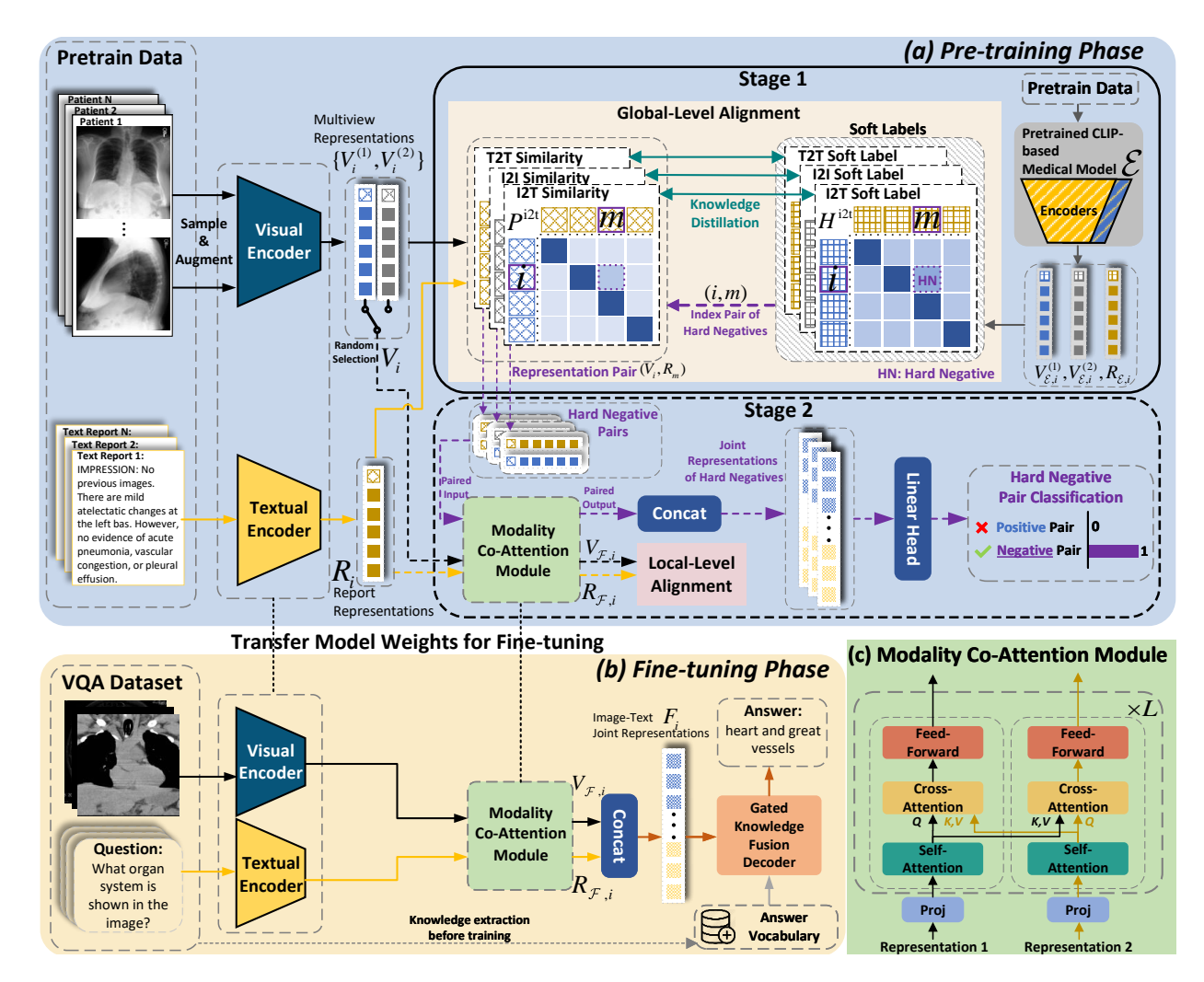


Figure 2. Architecture of AMiF: (a) Pre-Training Phase, (b) Fine-Tuning Phase, and (c) Modality Co-Attention Module.

Intra-Modality (**Multi-View & Text-Text**) For the multi-view images, the probability of aligning image $v_i^{(1)}$ and $v_i^{(2)}$ is computed as:

$$\begin{split} s_{ij}^{\text{i1,i2}} &= \text{proj}(\boldsymbol{v}_i^{(1)})^\top \text{proj}(\boldsymbol{v}_j^{(2)}), \\ P_{ij}^{\text{i1,i2}} &= \frac{\exp(s_{ij}^{\text{i1,i2}}/\tau_2)}{\sum_{k=1}^{N} \exp(s_{ik}^{\text{i1,i2}}/\tau_2)}. \end{split} \tag{3}$$

Similarly we obtain $P_{ij}^{\mathrm{i2,i1}}$. For text-text alignment, the probability of aligning report i and report j is computed as:

$$s_{ij}^{\text{t2t}} = \text{proj}(\boldsymbol{r}_i)^{\top} \text{proj}(\boldsymbol{r}_j),$$

$$P_{ij}^{\text{t2t}} = \frac{\exp(s_{ij}^{\text{t2t}}/\tau_3)}{\sum_{k=1}^{N} \exp(s_{ik}^{\text{t2t}}/\tau_3)}.$$
(4)

The τ_2 and τ_3 are temperature parameters.

Soft Label Generation We leverage a CLIP-based model [57] that is pre-trained on medical data to generate soft la-

bels for the inter-modality and intra-modality alignment. Denoting the multi-view image and text representations of the ith sample from the pre-trained CLIP-based model \mathcal{E} as $V_{\mathcal{E},i}^{(1)}, V_{\mathcal{E},i}^{(2)}$ and $R_{\mathcal{E},i}$, we use the embeddings of their [CLS] tokens as the global-level representations, yielding $v_{\mathcal{E},i}^{(1)}, v_{\mathcal{E},i}^{(2)}, r_{\mathcal{E},i} \in \mathbb{R}^d$. Afterward, following the same routines as Eqs. (2) to (4), we compute the softmax cosine similarities $Q_{ij}^{(2)}, Q_{ij}^{t2i}, Q_{ij}^{t2i}, Q_{ij}^{t2i,i1}, Q_{ij}^{t2i}, Q_{ij}^{t2t} \in \mathbb{R}$ based on $v_{\mathcal{E},i}^{(1)}, v_{\mathcal{E},i}^{(2)}$ and $r_{\mathcal{E},i}$. To add flexibility to the influence of positive image-text pairs and avoid classifying hard negatives as positive, we augment the soft labels by adding a flexibility weight λ for the positive pairs. Taking the soft label for inter-modality Q_{ij}^{i2t} as an example, we have the soft label computed as:

$$H_{ij}^{i2t} = Q_{ij}^{i2t} + \lambda \cdot \mathbf{1}_{\{i=i\}},$$
 (5)

The same augmentation applies to all other soft labels, generating $H^{\rm t2i}_{ij}, H^{\rm i1,i2}_{ij}, H^{\rm i2,i1}_{ij}$ and $H^{\rm t2t}_{ij}$.

Alignment with Soft Labels In contrastive learning, hard negatives are defined as negative image-text pairs with high similarities mistakenly. Since the one-hot label focuses on the positive image-text pair within the batch, the hard negatives are often overlooked. Instead of using one-hot labels and InfoNCE loss [42] as CLIP-based methods, we use soft labels for both inter-modality and intra-modality alignment. Specifically, We employ the knowledge distillation [19], comparing the similarity gained in Eqs. (2) to (4) with the corresponding soft labels from the pre-trained CLIP-based model $H_{ij}^{i2t}, H_{ij}^{t2i}, H_{ij}^{i1,i2}, H_{ij}^{i2,i1}, H_{ij}^{t2t} \in \mathbb{R}$. The knowledge distillation is achieved by minimizing the KL-divergence loss, computed as:

$$\mathcal{L}_{\text{inter}} = \frac{1}{2} \left(\mathcal{L}_{\text{inter}}^{\text{i2t}} + \mathcal{L}_{\text{inter}}^{\text{t2i}} \right)$$

$$= \frac{1}{2N} \sum_{i=1}^{N} \left(\text{KL}(H_i^{\text{i2t}} || P_i^{\text{i2t}}) + \text{KL}(H_i^{\text{t2i}} || P_i^{\text{t2i}}) \right),$$
(6)

where $P_i^{\mathrm{i}2\mathrm{t}} = \left[P_{i1}^{\mathrm{i}2\mathrm{t}}, \dots, P_{ij}^{\mathrm{i}2\mathrm{t}}, \dots, P_{iN}^{\mathrm{i}2\mathrm{t}}\right]$ denotes the probability distribution of aligning image i with all N possible reports, and the similar representation applies for $P_i^{\mathrm{t}2\mathrm{i}}, H_i^{\mathrm{i}2\mathrm{t}}$ and $H_i^{\mathrm{t}2\mathrm{i}}$. The loss for intra-modality alignment is:

$$\mathcal{L}_{\text{intra}} = \frac{1}{2} (\mathcal{L}_{\text{intra}}^{\text{i1},\text{i2}} + \mathcal{L}_{\text{intra}}^{\text{i2},\text{i1}}) + \mathcal{L}_{\text{intra}}^{\text{t2t}}$$

$$= \frac{1}{2N} \sum_{i=1}^{N} (\text{KL}(H_{i}^{\text{i1},\text{i2}} || P_{i}^{\text{i1},\text{i2}}) + \text{KL}(H_{i}^{\text{i2},\text{i1}} || P_{i}^{\text{i2},\text{i1}})) + \frac{1}{N} \sum_{i=1}^{N} \text{KL}(H_{i}^{\text{t2t}} || P_{i}^{\text{t2t}}).$$
(7)

For the first stage of pre-training, we conduct the globallevel alignment with the following total loss:

$$\mathcal{L}_{\text{global}} = \mathcal{L}_{\text{inter}} + \mathcal{L}_{\text{intra}}.$$
 (8)

3.2.2 Local-Level Alignment

In the second stage of pre-training, we first pass the multimodal representations V_i and R_i through a Modality Co-Attention Module (Fig. 2 (c)) that fuse each other's information, yielding the mutually-aware feature representations $V_{\mathcal{F},i}$ and $R_{\mathcal{F},i}$. Next, we align the p token embeddings of the image representation $V_{\mathcal{F},i} = \{v^1_{\mathcal{F},i}, v^2_{\mathcal{F},i}, \ldots, v^p_{\mathcal{F},i}\}$ with the t token embeddings of the report representation $R_{\mathcal{F},i} = \{r^1_{\mathcal{F},i}, r^2_{\mathcal{F},i}, \ldots, r^t_{\mathcal{F},i}\}$.

$$\begin{split} R_{\mathcal{F},i} &= \{ \boldsymbol{r}_{\mathcal{F},i}^1, \boldsymbol{r}_{\mathcal{F},i}^2, \dots, \boldsymbol{r}_{\mathcal{F},i}^{t^-} \}. \\ & \text{Our objective is to compute an optimal transport plan} \\ \mathbf{T} &\in \mathbb{R}^{p \times t} \text{ that minimizes the following loss function:} \end{split}$$

$$\mathcal{L}_{local} = \frac{1}{N} \sum_{i=1}^{N} \min_{\mathbf{T}} \sum_{i=1}^{p} \sum_{k=1}^{t} \mathbf{T}_{jk} \cdot C\left(\mathbf{v}_{\mathcal{F},i}^{j}, \mathbf{r}_{\mathcal{F},i}^{k}\right), \quad (9)$$

where $C(\cdot)$ is the cost function between two embeddings:

$$C\left(\boldsymbol{v}_{\mathcal{F},i}^{j},\boldsymbol{r}_{\mathcal{F},i}^{k}\right) = 1 - (\boldsymbol{v}_{\mathcal{F},i}^{j})^{\top}\boldsymbol{r}_{\mathcal{F},i}^{k}.$$
 (10)

Since minimizing the transport plan T directly is intractable, we use the inexact proximal point method (IPOT, [4, 8, 55]) to approximate an optimal transport plan T^* . The resulting optimal plan T^* captures how each image patch token is associated with a word token, based on the elements of the matrix.

3.3. Hard Negative Mining

The soft labels used for global-level alignment might compute high similarities to both hard negative pairs and positive pairs, which may lead to difficulties in distinguishing hard negative pairs from positive ones. We pair the representations of hard negatives from both inter-modality and intra-modality alignments, passing them through the Modality Co-Attention Module to generate mutually-aware representation pairs and enforce the classification on these representation pairs to be negative pairs, as illustrated in the lower-right of Fig. 2 (a).

Specifically, take the *i*-th sample for example, which consists of an image-text pair (V_i, R_i) used for its multimodality alignment. The distribution of I2T (image-text) soft labels for V_i is $H_i^{i2t} = [H_{i1}^{i2t}, \dots, H_{ij}^{i2t}, \dots, H_{iN}^{i2t}]$. We sample a hard negative pair (V_i, R_m) from H_i^{i2t} . The sampling rule is that a negative pair with higher similarity has a higher chance of being chosen. Based on the index pair (i, m) of the hard negative pair, where $m \neq i$, we pair (V_i, R_m) together, passing them to the Modality Co-Attention Module, resulting in a mutually-aware representation pair $(V_{\mathcal{F},i}, \mathbf{R}_{\mathcal{F},m})$. Similarly, for intra-modality alignment, we consider hard negative pairs within multi-view images and texts. For multi-view images, suppose that V_i of the i-th sample and V_n of the n-th sample $(n \neq i)$ form a hard negative pair. For texts, we have R_i and R_k forming a hard negative pair similarly, where $i \neq k$. Therefore, for the i-th sample, we build a hard negative set:

$$S_i^{\text{HN}} = \{ (V_{\mathcal{F},i}, R_{\mathcal{F},m}), (V_{\mathcal{F},i}, V_{\mathcal{F},n}), (R_{\mathcal{F},i}, R_{\mathcal{F},k}) \}. \tag{11}$$

Next, we formulate a classification problem to enforce the discrimination between hard negative pairs and positive pairs. Given representations of any hard negative pair $(a,b) \in \mathcal{S}_i^{\mathrm{HN}}$, we first concatenate (Concat) these two representations, forming a joint representation. Then, a linear classification head (LH) is applied to this joint representation, which outputs a prediction logits:

$$p_{(a,b)} = LH(Concat(a,b)).$$
 (12)

A cross-entropy (CE) loss is applied on classifying hard negative pairs using Eq. (12):

$$\mathcal{L}_{HN} = \frac{1}{N} \sum_{i=1}^{N} \sum_{(\boldsymbol{a}, \boldsymbol{b}) \in \mathcal{S}_{i}^{HN}} CE(\boldsymbol{p}_{(\boldsymbol{a}, \boldsymbol{b})}; y_{(\boldsymbol{a}, \boldsymbol{b})}), \qquad (13)$$

where $y_{(a,b)}$ is a one-hot label (the hard negative pair is assigned with label 1 while the positive pair with label 0).

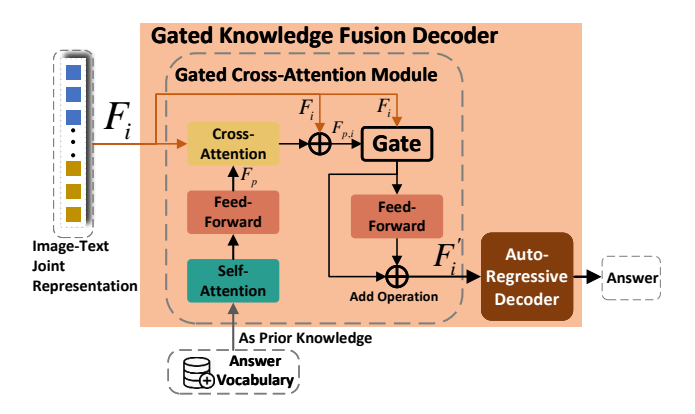


Figure 3. Architecture of Gated Knowledge Fusion Decoder, which consists of a Gated Cross-Attention Module and an Auto-Regressive Decoder.

3.4. Gated Knowledge Fusion Decoder

To fine-tune the model pre-trained by the alignment and hard negative mining for specific downstream tasks such as Med-VQA (Fig. 2 (b)), we design a Gated Knowledge Fusion Decoder (Fig. 3), which consists of (1) a Gated Cross-Attention Module to select related knowledge from the generic prior knowledge and fuse it into the domain-specific downstream task; and (2) an auto-regressive decoder to generate *open*-form answers.

3.4.1 Gated Cross-Attention Module

Generic prior knowledge usually contains comprehensive information covering a wide range of medical topics, so irrelevant information is involved when applied to a specific-field Med-VQA task. Thus, we propose a Gated Cross-Attention Module (Fig. 3), which fuses the prior knowledge into the input image-question representation and uses a gate operation to select relevant information from the knowledge-fused representation.

Given an image-text joint representation $F_i \in \mathbb{R}^{(p+t) \times d}$, where p,t are the token numbers for image and text representations. We input it into the Gated Cross-Attention Module. The generic prior knowledge is represented by an answer vocabulary extracted from the Med-VQA dataset for fine-tuning, which is passed through a self-attention and a feed-forward sub-module, yielding $F_p \in \mathbb{R}^{M \times d}$, where M is the total token length of the knowledge. We use cross-attention for fusing the prior knowledge F_p and joint representation F_i . Specifically, the knowledge-fused representation is computed as:

$$F_{p,i} = \operatorname{CA}(F_i, F_p) + F_i, \tag{14}$$

where $CA(\cdot)$ represents the cross-attention mechanism, with the first argument as the query (Q), and the second as the key (K) and value (V).

Next, to select related information from prior knowledge for accurate answer prediction, we have:

$$G_{p,i} = \text{Sigmoid}(\text{Projection}(F_{p,i})),$$
 (15)

where $\operatorname{Sigmoid}(\cdot)$ is an activation function and $\operatorname{Projection}(\cdot)$ is a mapping function in the d-dimensional space. The resulting $G_{p,i} \in \mathbb{R}^{(p+t)\times d}$ is a weight matrix with all values between 0 and 1, indicating the portion of information selected from knowledge fused representation $F_{p,i}$. To balance information from the knowledge-fused representation $F_{p,i}$ and the image-text joint representation F_i , we have the gated operation in Fig. 3 formulated as:

$$Gate(F_{p,i}, F_i) = G_{p,i} \odot F_{p,i} + (1 - G_{p,i}) \odot F_i,$$
 (16)

where \odot is the element-wise product. The representation $\operatorname{Gate}(F_{p,i},F_i)$ is then passed through a feed-forward sub-module, yielding a final knowledge-fused image-question representation F_i' for the answer generation below.

3.4.2 Auto-Regressive Decoder

Different from prior methods like [9, 10, 30] that predict answers by classifying from a fixed answer list, we utilize an auto-regressive decoder [11, 28] to generate *open*-form answers. Given the selected knowledge-fused image-question representation F'_i from Sec. 3.4.1, the decoder is trained to generate answers auto-regressively via a conditional language modeling loss.

4. Experiment

4.1. Datasets

Pre-training Datasets For pre-training AMiF, we use three medical datasets that are widely used for Med-VLP: MIMIC-CXR [24] is the largest publicly available radiology dataset that contains 377110 X-ray chest images and 227827 corresponding reports; ROCO [43] is a radiology dataset that has over 81,000 radiology images from various imaging modalities and their corresponding captions; and MedICaT [49] is a medical figure-caption dataset that contains over 217,000 image-caption pairs.

Multi-view Images For MIMIC-CXR, there are existing multi-view images for each radiology study, so we randomly sample two different views. For ROCO and Med-ICaT datasets, which lack the multi-view information for each sample, we apply strong random data augmentation [6] for generating multi-views from one image. Ultimately we ensure all samples from the datasets have two multi-view images for intra-modality (image-image) alignment.

Method	VQA-RAD			SLAKE			PathVQA			VQA2019
Method	Open	Closed	Overall	Open	Closed	Overall	Open	Closed	Overall	Overall
MMQ [13]	53.70	75.80	67.00	-	-	-	13.40	84.0	48.80	-
MEVF-BAN [41]	49.20	77.20	66.10	77.80	79.80	78.60	-	-	-	77.86
CPRD [35]	52.50	77.90	67.80	79.50	83.40	81.10	-	-	-	-
MMBERT [25]	63.10	77.90	72.00	-	-	-	-	-	-	67.20
ARL [10]	65.10	85.96	77.50	79.70	89.30	84.00	-	-	-	80.32
M3AE [9]	67.23	83.46	77.01	80.31	87.82	83.25	-	-	-	79.87
PubMedCLIP [15]	60.10	80.00	72.10	78.40	82.50	80.10	-	-	-	-
CPCR [37]	60.50	80.40	72.50	80.50	84.10	81.90	-	-	-	-
M2I2 [30]	61.80	81.60	73.70	74.70	91.10	81.20	36.30	88.00	62.20	-
MUMC [29]	<u>71.50</u>	84.20	79.20	-	-	84.90	<u>39.00</u>	90.40	<u>65.10</u>	-
RAMM [56]	-	-	78.27	-	-	<u>86.05</u>	-	-	-	82.13
PeFoMed [17]	62.60	<u>87.10</u>	77.40	77.80	88.70	82.10	35.70	91.30	63.60	-
LaPA [16]	68.72	86.40	79.38	82.17	88.70	84.73	-	-	-	81.60
BiomedCLIP [57]	67.60	79.80	75.20	82.50	89.70	85.40	-	-	-	-
AMiF(Ours)	72.00	87.25	80.49	84.84	90.23	86.71	40.33	90.18	65.33	83.20

Table 1. Accuracy comparison with existing methods on various VQA datasets, evaluated for *Open* and *Closed* sets and the *Overall* performances. *Open* represents a question set with *open*-form answers while *Closed* represents the question set with *yes/no* as the answer. The best and second-best results are **bolded** and <u>underlined</u> respectively.

Med-VQA Datasets for Fine-tuning For fine-tuning the model for the Med-VQA task, we use VQA-RAD [27], SLAKE [36], VQA-2019 [2] and PathVQA[18]. VQA-RAD has 315 radiology images with 3064 question-answer pairs. SLAKE has 14,028 pairs of samples. VQA-2019 comprises 15,292 question-answer pairs. PathVQA contains 32,799 question-answer pairs. All datasets contain *Open* set (open-form answers) and *Closed* set (*yes/no* answers), and we follow the official splits for all datasets.

4.2. Implementation Details

For the pre-training phase, we apply CLIP-ViT/B-16 [46] as the initialized visual encoder, and ClinicalBERT [21] as the initialized textual encoder and decoder. For the fine-tuning phase, the Modality Co-Attention Module uses L=6 layers. The temperature parameters τ_1,τ_2,τ_3 are set to 0.07. The flexibility weight of the positive pair λ is set to 0.01. The total trainable model size is 326M, while the size of Gated Cross-Attention Module are 14.8M.

Our pre-training phase contains 20 epochs for stage one, and 10 epochs for stage two, with 256 as batch size. The model uses AdamW optimizer with a learning rate of 4e-6.

For more details about the implementation and training, please refer to the Supplement.

4.3. Comparison with the State-of-the-Art

As shown in Tab. 1, our method outperforms other methods across all Med-VQA datasets for *Overall* accuracy, and for the *Open* type questions, which is more challenging than *Closed* type, we also achieve the best performance. Notably, compared with BiomedCLIP [57], which is the pretrained model we utilize to generate soft labels, our method

surpasses it on VQA-RAD and SLAKE datasets by 5.29% and 1.31% separately. For the PathVQA dataset, which is the largest one with challenging open-form question-answer pairs, we outperform the second best by 1.33%. These results show that our method has a better understanding ability on the Med-VQA tasks, with room for improvements.

4.4. Ablation Study

Ablation for Unified Modality Alignment To explore the impact of different components for pre-training, we conduct systematic ablative experiments for unified modality alignments in Tab. 2. Notably, our baseline (#1) only uses global inter-modality alignment. To prove the significance of intra-modality alignment to our AMiF, we conduct ablations #3, #7, and #8, which show improvements in average accuracy compared with #1, #5, and #6, respectively. When applying intra-modality alignment, we also evaluate the effectiveness of multi-view alignment via #3, which elevates the average accuracy by 0.78% compared with only texttext alignment (#2). To demonstrate that local-level alignment improves the model's ability, we compare #4 with #3, which shows a 0.90% increase in accuracy. Moreover, We also evaluate the impact of different weight combination in stage 2 of pre-training (i.e., local-level alignment loss and hard-negative mining loss), as shown in Tab. 3. Based on the ablative results we choose to balance those two losses.

Ablation for Hard Negative Mining To show that our approach of hard negative mining benefits model performance on Med-VQA tasks, we first investigate the necessity of using soft labels for global-level alignment. As shown in

#	G-inter	G-intra	Local	Soft Label	HN	RAD-VQA	SLAKE	Path-VQA	VQA-2019	Avg
1	√					76.68	82.4	61.23	79.06	74.84
2	✓	*				77.06	82.47	61.92	79.70	75.28
3	✓	✓				77.92	82.64	63.78	79.88	76.06
4	✓	✓	✓			78.44	83.83	64.66	80.92	76.96
5	✓		✓	✓		79.04	85.98	65.24	81.34	77.90
6	✓		✓	✓	✓	79.77	86.20	65.30	81.83	78.28
7	✓	✓	✓	✓		79.82	86.07	65.21	82.21	78.33
8	/	1	1	✓	✓	80.49	86.71	65.33	83.20	78.93

Table 2. Ablation study for pre-training using different components (\checkmark). G-inter and G-intra denote global inter- and intra-modality alignments, respectively. For intra-modality, * denotes only text-text alignment, while \checkmark denotes both multi-view and text-text alignments. Local denotes local-level alignment. Soft Label denotes soft label for global-level alignment and HN denotes hard negative mining.

#	$\mathcal{L}_{\mathrm{local}}$	$\mathcal{L}_{\mathrm{HN}}$	RAD-VQA	SLAKE	Path-VQA	VQA-2019	Avg
1	1.0	1.0	80.49	86.71	65.33	83.20	78.93
2	1.0	0.2	78.32	84.92	63.30	82.15	77.17
3	0.2	1.0	79.57	84.82	64.93	82.53	77.96
4	1.0	3.0	79.16	85.17	64.46	82.26	77.76
5	3.0	1.0	78.61	84.59	65.42	83.14	77.94

Table 3. Ablation study for pertaining with different weight combinations of Hard Negative Mining Loss (HN) and Local-Level Alignment Loss (local).

#	Pre-training	Knowledge	RAD-VQA	SLAKE	Path-VQA	VQA-2019	Avg
1	-	-	75.64	81.09	60.92	78.14	73.95
2	CLIP-based	-	77.65	82.92	61.30	79.92	75.45
3	Ours	-	79.03	84.32	63.53	81.03	76.98
4	Ours	Q	79.55	85.04	63.93	82.13	77.36
5	Ours	A	80.26	85.37	63.96	81.26	77.71
6	Ours	A&G	80.49	86.71	65.33	83.20	78.93

Table 4. Ablation study for fine-tuning on Med-VQA task. $\bf Q$ and $\bf A$ denotes introducing question and answer vocabulary as prior Knowledge, respectively. $\bf G$ denotes using the Gated operation in the Gated Cross-Attention Module.

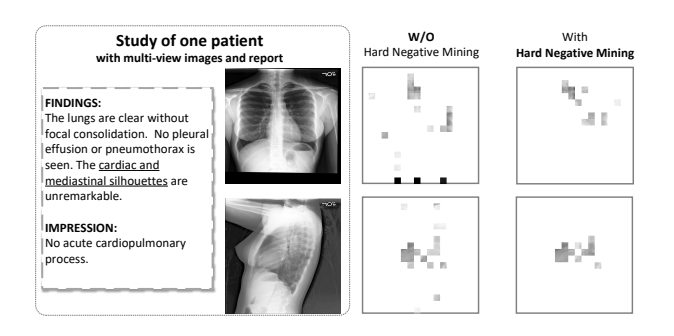


Figure 4. Visualization of the local-level alignment related to <u>underlined</u> words for the ablative study of hard negative mining.

Tab. 2, the comparison between #7 and #4 indicates that using soft labels boosts the average model performance by 1.37%. We also show that soft labels for global intra-modality alignment facilitates the model's representation ability by comparing #7 with #5. Moreover, to prove the significance of hard negative pair discrimination, we compare #6 with #5 and #8 with #7. Besides, we also conduct a qualitative ablation study for hard negative mining as shown in Fig. 4, comparing ablations #8 and #4. After hard negative mining, the patch tokens related to the underlined words are more concentrated on regions with possible semantic information, showing that our mining method leads to a more robust modality co-attention module, which yields more interpretable results for local-level alignment.

Ablation for Fine-tuning Med-VQA In Tab. 4, we show that compared with training our model from scratch (#1), our pre-training method (#3) greatly improves the average accuracy by 3.03%. The comparison between #3 and #2 shows that our pre-training method outperforms the CLIP-based model [57] used for generating soft labels. Besides the pre-training method, we study how selective knowledge fusion facilitates Med-VQA tasks. Comparing #4

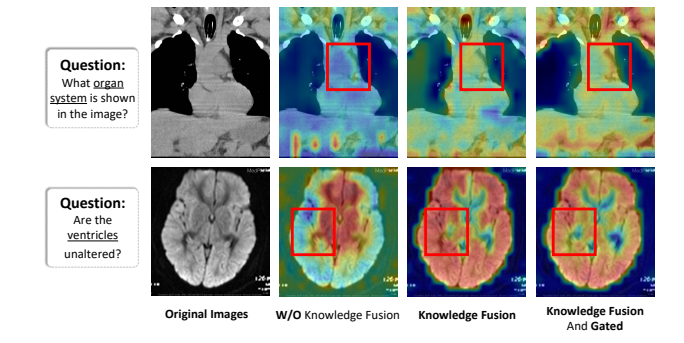


Figure 5. Attention map related to <u>underlined</u> words for the ablative study of selective knowledge fusion.

with #3, we find that fusing <u>question vocabulary</u> to image-question representation improves the model performance for question-answering by 0.38%. When we fuse the <u>answer vocabulary</u> instead (#5), we find the average performance is raised by 0.35%. These results are further enhanced when we apply the gated operation in our <u>Gated Cross-Attention Module</u> (#6), improving the average accuracy by 1.22% based on #5, which is the best result we currently have. Additionally, we visualize the attention map in Fig. 5. From regions denoted with red boxes, we see that the gated operation selects relevant information and filters out unnecessary ones.

5. Conclusion

In this paper, we introduced AMiF to address the challenges in Medical Visual Question Answering (Med-VQA). Specifically, we propose solutions for unified modality Alignment, hard negative Mining, and selective knowledge Fusion. We unify heterogeneous modality alignments across multiple levels, modalities, views, and stages. Our hard negative mining method employs soft labels for both inter-modality and intra-modality alignments and explores hard negative pairs to distinguish them from positive ones via enforced discrimination. For the Med-VQA task, we introduce a Gated Cross-Attention Module that integrates the answer vocabulary as prior knowledge and selects relevant information from it. Our experiments demonstrate the effectiveness of our approach on Med-VQA tasks, compared with the previous state-of-the-art.

References

- [1] Alex Andonian, Shixing Chen, and Raffay Hamid. Robust cross-modal representation learning with progressive selfdistillation. In *Proceedings of the IEEE/CVF Conference* on Computer Vision and Pattern Recognition, pages 16430– 16441, 2022. 3
- [2] Asma Ben Abacha, Sadid A Hasan, Vivek V Datla, Dina Demner-Fushman, and Henning Müller. Vqa-med: Overview of the medical visual question answering task at imageclef 2019. In *Proceedings of CLEF (Conference and Labs of the Evaluation Forum) 2019 Working Notes*. 9-12 September 2019, 2019. 2, 7
- [3] Olivier Bodenreider. The unified medical language system (umls): integrating biomedical terminology. *Nucleic acids research*, 32(suppl_1):D267–D270, 2004. 2
- [4] Stephen Boyd and Lieven Vandenberghe. *Convex optimization*. Cambridge university press, 2004. 5
- [5] Cheng Chen, Aoxiao Zhong, Dufan Wu, Jie Luo, and Quanzheng Li. Contrastive masked image-text modeling for medical visual representation learning. In *International Conference on Medical Image Computing and Computer-Assisted Intervention*, pages 493–503. Springer, 2023. 1, 2,
- [6] Ting Chen, Simon Kornblith, Mohammad Norouzi, and Geoffrey Hinton. A simple framework for contrastive learning of visual representations. In *International conference on machine learning*, pages 1597–1607. PMLR, 2020. 1, 6
- [7] Xiaofei Chen, Yuting He, Cheng Xue, Rongjun Ge, Shuo Li, and Guanyu Yang. Knowledge boosting: Rethinking medical contrastive vision-language pre-training. In *International Conference on Medical Image Computing and Computer-Assisted Intervention*, pages 405–415. Springer, 2023. 1, 3
- [8] Yen-Chun Chen, Linjie Li, Licheng Yu, Ahmed El Kholy, Faisal Ahmed, Zhe Gan, Yu Cheng, and Jingjing Liu. Uniter: Universal image-text representation learning. In *European conference on computer vision*, pages 104–120. Springer, 2020. 3, 5
- [9] Zhihong Chen, Yuhao Du, Jinpeng Hu, Yang Liu, Guanbin Li, Xiang Wan, and Tsung-Hui Chang. Multi-modal masked autoencoders for medical vision-and-language pretraining. In *International Conference on Medical Image Computing and Computer-Assisted Intervention*, pages 679– 689. Springer, 2022. 1, 3, 6, 7
- [10] Zhihong Chen, Guanbin Li, and Xiang Wan. Align, reason and learn: Enhancing medical vision-and-language pretraining with knowledge. In *Proceedings of the 30th ACM International Conference on Multimedia*, pages 5152–5161, 2022. 1, 2, 3, 6, 7
- [11] Jaemin Cho, Jie Lei, Hao Tan, and Mohit Bansal. Unifying vision-and-language tasks via text generation. In *Interna*tional Conference on Machine Learning, pages 1931–1942. PMLR, 2021. 6
- [12] Gefen Dawidowicz, Elad Hirsch, and Ayellet Tal. Limitr: Leveraging local information for medical image-text representation. In *Proceedings of the IEEE/CVF International*

- Conference on Computer Vision, pages 21165–21173, 2023. 1, 3
- [13] Tuong Do, Binh X Nguyen, Erman Tjiputra, Minh Tran, Quang D Tran, and Anh Nguyen. Multiple meta-model quantifying for medical visual question answering. In Medical Image Computing and Computer Assisted Intervention— MICCAI 2021: 24th International Conference, Strasbourg, France, September 27—October 1, 2021, Proceedings, Part V 24, pages 64–74. Springer, 2021. 2, 3, 7
- [14] Li Dong, Nan Yang, Wenhui Wang, Furu Wei, Xiaodong Liu, Yu Wang, Jianfeng Gao, Ming Zhou, and Hsiao-Wuen Hon. Unified language model pre-training for natural language understanding and generation. Advances in neural information processing systems, 32, 2019. 3
- [15] Sedigheh Eslami, Christoph Meinel, and Gerard De Melo. Pubmedclip: How much does clip benefit visual question answering in the medical domain? In *Findings of the Association for Computational Linguistics: EACL 2023*, pages 1181–1193, 2023. 1, 2, 3, 7
- [16] Tiancheng Gu, Kaicheng Yang, Dongnan Liu, and Weidong Cai. Lapa: Latent prompt assist model for medical visual question answering. In Proceedings of the IEEE/CVF Conference on Computer Vision and Pattern Recognition (CVPR) Workshops, 2024. 1, 2, 3, 7
- [17] Jinlong He, Pengfei Li, Gang Liu, Zixu Zhao, and Shenjun Zhong. Pefomed: Parameter efficient fine-tuning on multimodal large language models for medical visual question answering. *arXiv preprint arXiv:2401.02797*, 2024. 7
- [18] Xuehai He. Towards visual question answering on pathology images. In *Proceedings of the 59th annual meeting of the association for computational linguistics and the 11th international joint conference on natural language processing*, 2021. 2, 7
- [19] Geoffrey Hinton, Oriol Vinyals, and Jeff Dean. Distilling the knowledge in a neural network. arXiv preprint arXiv:1503.02531, 2015. 5
- [20] Hailang Huang, Zhijie Nie, Ziqiao Wang, and Ziyu Shang. Cross-modal and uni-modal soft-label alignment for imagetext retrieval. In *Proceedings of the AAAI Conference on Artificial Intelligence*, pages 18298–18306, 2024. 3
- [21] Kexin Huang, Jaan Altosaar, and Rajesh Ranganath. Clinicalbert: Modeling clinical notes and predicting hospital readmission. *arXiv preprint arXiv:1904.05342*, 2019. 7, 1
- [22] Shih-Cheng Huang, Liyue Shen, Matthew P Lungren, and Serena Yeung. Gloria: A multimodal global-local representation learning framework for label-efficient medical image recognition. In *Proceedings of the IEEE/CVF International* Conference on Computer Vision, pages 3942–3951, 2021. 1, 2
- [23] Jongseong Jang, Daeun Kyung, Seung Hwan Kim, Honglak Lee, Kyunghoon Bae, and Edward Choi. Significantly improving zero-shot x-ray pathology classification via finetuning pre-trained image-text encoders. *Scientific Reports*, 14(1):23199, 2024. 3
- [24] Alistair EW Johnson, Tom J Pollard, Nathaniel R Greenbaum, Matthew P Lungren, Chih-ying Deng, Yifan Peng, Zhiyong Lu, Roger G Mark, Seth J Berkowitz, and Steven

- Horng. Mimic-cxr-jpg, a large publicly available database of labeled chest radiographs. *arXiv preprint arXiv:1901.07042*, 2019. 1, 6
- [25] Yash Khare, Viraj Bagal, Minesh Mathew, Adithi Devi, U Deva Priyakumar, and CV Jawahar. Mmbert: Multimodal bert pretraining for improved medical vqa. In 2021 IEEE 18th International Symposium on Biomedical Imaging (ISBI), pages 1033–1036. IEEE, 2021. 7
- [26] Wonjae Kim, Bokyung Son, and Ildoo Kim. Vilt: Visionand-language transformer without convolution or region supervision. In *Proceedings of the 38th International Conference on Machine Learning*, pages 5583–5594. PMLR, 2021.
- [27] Jason J Lau, Soumya Gayen, Asma Ben Abacha, and Dina Demner-Fushman. A dataset of clinically generated visual questions and answers about radiology images. *Scientific* data, 5(1):1–10, 2018. 2, 7
- [28] Junnan Li, Ramprasaath Selvaraju, Akhilesh Gotmare, Shafiq Joty, Caiming Xiong, and Steven Chu Hong Hoi. Align before fuse: Vision and language representation learning with momentum distillation. Advances in neural information processing systems, 34:9694–9705, 2021. 3, 6
- [29] Pengfei Li, Gang Liu, Jinlong He, Zixu Zhao, and Shenjun Zhong. Masked vision and language pre-training with unimodal and multimodal contrastive losses for medical visual question answering. In *International Conference on Medical Image Computing and Computer-Assisted Intervention*, pages 374–383. Springer, 2023. 1, 2, 3, 7
- [30] Pengfei Li, Gang Liu, Lin Tan, Jinying Liao, and Shenjun Zhong. Self-supervised vision-language pretraining for medial visual question answering. In 2023 IEEE 20th International Symposium on Biomedical Imaging (ISBI), pages 1–5, 2023. 1, 2, 3, 6, 7
- [31] Ruizhi Liao, Daniel Moyer, Miriam Cha, Keegan Quigley, Seth Berkowitz, Steven Horng, Polina Golland, and William M Wells. Multimodal representation learning via maximization of local mutual information. In Medical Image Computing and Computer Assisted Intervention–MICCAI 2021: 24th International Conference, Strasbourg, France, September 27–October 1, 2021, Proceedings, Part II 24, pages 273–283. Springer, 2021. 2
- [32] Weixiong Lin, Ziheng Zhao, Xiaoman Zhang, Chaoyi Wu, Ya Zhang, Yanfeng Wang, and Weidi Xie. Pmc-clip: Contrastive language-image pre-training using biomedical documents. In *International Conference on Medical Image Com*puting and Computer-Assisted Intervention, pages 525–536. Springer, 2023. 1
- [33] Zudi Lin, Erhan Bas, Kunwar Yashraj Singh, Gurumurthy Swaminathan, and Rahul Bhotika. Relaxing contrastiveness in multimodal representation learning. In *Proceedings of the IEEE/CVF winter conference on applications of computer vision*, pages 2227–2236, 2023. 1, 3
- [34] Zhihong Lin, Donghao Zhang, Qingyi Tao, Danli Shi, Gholamreza Haffari, Qi Wu, Mingguang He, and Zongyuan Ge. Medical visual question answering: A survey. Artificial Intelligence in Medicine, 143:102611, 2023.
- [35] Bo Liu, Li-Ming Zhan, and Xiao-Ming Wu. Contrastive pre-training and representation distillation for medical visual

- question answering based on radiology images. In Medical Image Computing and Computer Assisted Intervention—MICCAI 2021: 24th International Conference, Strasbourg, France, September 27—October 1, 2021, Proceedings, Part II 24, pages 210–220. Springer, 2021. 3, 7
- [36] Bo Liu, Li-Ming Zhan, Li Xu, Lin Ma, Yan Yang, and Xiao-Ming Wu. Slake: A semantically-labeled knowledgeenhanced dataset for medical visual question answering. In 2021 IEEE 18th International Symposium on Biomedical Imaging (ISBI), pages 1650–1654. IEEE, 2021. 2, 7
- [37] Bo Liu, Li-Ming Zhan, Li Xu, and Xiao-Ming Wu. Medical visual question answering via conditional reasoning and contrastive learning. *IEEE transactions on medical imaging*, 42(5):1532–1545, 2022. 7
- [38] Yunyi Liu, Zhanyu Wang, Dong Xu, and Luping Zhou. Q2atransformer: Improving medical vqa via an answer querying decoder. In *International Conference on Information Processing in Medical Imaging*, pages 445–456. Springer, 2023. 3
- [39] Sruthy Manmadhan and Binsu C Kovoor. Visual question answering: a state-of-the-art review. Artificial Intelligence Review, 53(8):5705–5745, 2020. 1
- [40] Philip Müller, Georgios Kaissis, Congyu Zou, and Daniel Rueckert. Joint learning of localized representations from medical images and reports. In *European Conference on Computer Vision*, pages 685–701. Springer, 2022. 1, 3
- [41] Binh D Nguyen, Thanh-Toan Do, Binh X Nguyen, Tuong Do, Erman Tjiputra, and Quang D Tran. Overcoming data limitation in medical visual question answering. In Medical Image Computing and Computer Assisted Intervention— MICCAI 2019: 22nd International Conference, Shenzhen, China, October 13–17, 2019, Proceedings, Part IV 22, pages 522–530. Springer, 2019. 2, 3, 7
- [42] Aaron van den Oord, Yazhe Li, and Oriol Vinyals. Representation learning with contrastive predictive coding. *arXiv* preprint arXiv:1807.03748, 2018. 5
- [43] Obioma Pelka, Sven Koitka, Johannes Rückert, Felix Nensa, and Christoph M Friedrich. Radiology objects in context (roco): a multimodal image dataset. In Intravascular Imaging and Computer Assisted Stenting and Large-Scale Annotation of Biomedical Data and Expert Label Synthesis: 7th Joint International Workshop, CVII-STENT 2018 and Third International Workshop, LABELS 2018, Held in Conjunction with MICCAI 2018, Granada, Spain, September 16, 2018, Proceedings 3, pages 180–189. Springer, 2018. 6
- [44] Matthew E Peters, Mark Neumann, Robert L Logan IV, Roy Schwartz, Vidur Joshi, Sameer Singh, and Noah A Smith. Knowledge enhanced contextual word representations. arXiv preprint arXiv:1909.04164, 2019.
- [45] Filip Radenovic, Abhimanyu Dubey, Abhishek Kadian, Todor Mihaylov, Simon Vandenhende, Yash Patel, Yi Wen, Vignesh Ramanathan, and Dhruv Mahajan. Filtering, distillation, and hard negatives for vision-language pre-training. In Proceedings of the IEEE/CVF conference on computer vision and pattern recognition, pages 6967–6977, 2023. 3
- [46] Alec Radford, Jong Wook Kim, Chris Hallacy, Aditya Ramesh, Gabriel Goh, Sandhini Agarwal, Girish Sastry,

- Amanda Askell, Pamela Mishkin, Jack Clark, et al. Learning transferable visual models from natural language supervision. In *International conference on machine learning*, pages 8748–8763. PMLR, 2021. 1, 7
- [47] Syed A Rizvi, Ruixiang Tang, Xiaoqian Jiang, Xiaotian Ma, and Xia Hu. Local contrastive learning for medical image recognition. In AMIA Annual Symposium Proceedings, page 1236. American Medical Informatics Association, 2023. 2
- [48] Prashant Shrestha, Sanskar Amgain, Bidur Khanal, Cristian A Linte, and Binod Bhattarai. Medical vision language pretraining: A survey. arXiv preprint arXiv:2312.06224, 2023. 3
- [49] Sanjay Subramanian, Lucy Lu Wang, Sachin Mehta, Ben Bogin, Madeleine van Zuylen, Sravanthi Parasa, Sameer Singh, Matt Gardner, and Hannaneh Hajishirzi. Medicat: A dataset of medical images, captions, and textual references. arXiv preprint arXiv:2010.06000, 2020. 6
- [50] Tim Tanida, Philip Müller, Georgios Kaissis, and Daniel Rueckert. Interactive and explainable region-guided radiology report generation. In *Proceedings of the IEEE/CVF Conference on Computer Vision and Pattern Recognition*, pages 7433–7442, 2023. 1
- [51] Petar Veličković, Guillem Cucurull, Arantxa Casanova, Adriana Romero, Pietro Lio, and Yoshua Bengio. Graph attention networks. arXiv preprint arXiv:1710.10903, 2017.
- [52] Fuying Wang, Yuyin Zhou, Shujun Wang, Varut Vardhanabhuti, and Lequan Yu. Multi-granularity cross-modal alignment for generalized medical visual representation learning. Advances in Neural Information Processing Systems, 35:33536–33549, 2022. 1, 3
- [53] Xiaozhi Wang, Tianyu Gao, Zhaocheng Zhu, Zhengyan Zhang, Zhiyuan Liu, Juanzi Li, and Jian Tang. Kepler: A unified model for knowledge embedding and pre-trained language representation. *Transactions of the Association for Computational Linguistics*, 9:176–194, 2021. 2
- [54] Zifeng Wang, Zhenbang Wu, Dinesh Agarwal, and Jimeng Sun. Medclip: Contrastive learning from unpaired medical images and text. arXiv preprint arXiv:2210.10163, 2022. 1, 2, 3
- [55] Yujia Xie, Xiangfeng Wang, Ruijia Wang, and Hongyuan Zha. A fast proximal point method for computing exact wasserstein distance. In *Uncertainty in artificial intelligence*, pages 433–453. PMLR, 2020. 3, 5
- [56] Zheng Yuan, Qiao Jin, Chuanqi Tan, Zhengyun Zhao, Hongyi Yuan, Fei Huang, and Songfang Huang. Ramm: Retrieval-augmented biomedical visual question answering with multi-modal pre-training. In *Proceedings of the 31st ACM International Conference on Multimedia*, pages 547–556, 2023. 7
- [57] Sheng Zhang, Yanbo Xu, Naoto Usuyama, Hanwen Xu, Jaspreet Bagga, Robert Tinn, Sam Preston, Rajesh Rao, Mu Wei, Naveen Valluri, et al. Biomedclip: a multimodal biomedical foundation model pretrained from fifteen million scientific image-text pairs. arXiv preprint arXiv:2303.00915, 2023. 1, 2, 3, 4, 7, 8
- [58] Yuhao Zhang, Hang Jiang, Yasuhide Miura, Christopher D Manning, and Curtis P Langlotz. Contrastive learning of

- medical visual representations from paired images and text. In *Machine Learning for Healthcare Conference*, pages 2–25. PMLR, 2022. 1
- [59] Hong-Yu Zhou, Chenyu Lian, Liansheng Wang, and Yizhou Yu. Advancing radiograph representation learning with masked record modeling. arXiv preprint arXiv:2301.13155, 2023. 1, 2, 3

Alignment, Mining and Fusion: Representation Alignment with Hard Negative Mining and Selective Knowledge Fusion for Medical Visual Question Answering

Supplementary Material

6. Implementation Details

For the pre-training phase, we apply CLIP-ViT/B-16 [46] as the initialized visual encoder, and ClinicalBERT [21] as the initialized textual encoder and auto-regressive decoder. All images are resized to 288×288. The dimension of embeddings d is set to 768. The Modality Co-Attention Module uses L=6 layers. The total trainable model size is 326M. The temperature parameters τ_1, τ_2, τ_3 are set to 0.07. The flexibility weight of the positive pair is cross-validated among different value choices and set $\lambda=0.01$. Our pretraining phase contains 20 epochs for stage one, and 10 epochs for stage two, with 256 as batch size. The model uses AdamW optimizer with a learning rate of 4e-6.

For the fine-tuning phase, the parameters for the Gated Cross-Attention Module are 14.8M, while 122M for the auto-regressive decoder. We fine-tune the model for 60 epochs with a learning rate of 2e-5 and a batch size of 64.

Our computing resources are two NVIDIA A100 GPUs, and the training uses 16-mixed precision. The pre-training costs roughly 24 hours, while fine-tuning time is around 8 hours. The inference time for one image-question pair is around 0.27s. During inference, to fairly compare with other multi-label classification-based methods, we apply the test set answers as the candidate answers, compare the generated open-form answer from our auto-regressive decoder with these candidates, and choose the one with the lowest language modeling loss.

7. Additive Ablation Studies

Besides the ablation study we conduct in Sec. 4.4, we also evaluate the impacts of different methods we use to generate the soft labels, and how the λ (Eq. (5)) will affect the learning of these soft labels.

#	Soft Label Generation Method	RAD-VQA	SLAKE	Path-VQA	VQA-2019	Avg
1	=	75.64	81.09	60.92	78.14	73.95
2	CLIP[46]	76.35	81.32	61.38	78.42	74.37
3	MedCLIP [54]	78.80	84.82	62.83	81.03	76.87
4	PubMedCLIP[15]	80.02	85.32	63.12	80.93	77.35
5	PMC-CLIP[32]	79.63	84.98	63.01	80.44	77.02
6	BioMedCLIP [57]	80.26	85.37	63.96	81.26	77.71

Table 5. Ablation study on different choices of soft label generation methods for Med-VQA tasks.

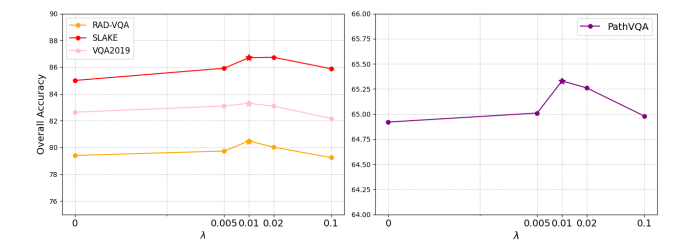


Figure 6. Ablation study on different choices of flexibility weight λ for Med-VQA tasks. Datasets are split based on the range of accuracy values.

7.1. Impacts of Different Soft Label Generation Methods

During our experiment for exploring soft label generation, we attempt different CLIP-based models, evaluating their performances in depicting the similarity between imagetext pairs. Our ablative experiment focuses on several representative CLIP-based models [15, 32, 46, 54, 57]. We use the base version of these models to keep all model sizes in a comparative range.

As shown in Tab. 5, when we focus on the average accuracy, the comparison between #2 (CLIP [46]) and the best one #6 (BioMedCLIP [57]) indicates that soft labels generated from the medical-specific model have better instructional impacts than the model from natural domain. While #4, #5, #6 are all models pre-trained on medical datasets, the average results are close to each other, which demonstrates that the usage of medical knowledge has a nearly equal effect on improving the model representation ability for Med-VQA tasks. In conclusion, we believe a well-trained CLIP-based model in medical domain will benefit the soft label supervision, and thus improving the performance of downstream tasks (*e.g.*, Med-VQA).

7.2. Impacts of flexibility weight λ for soft labels

We also evaluate different settings of λ that control the positive sample's similarity, and we find out that $\lambda=0.01$ is a locally best choice, as shown in Fig. 6. Our explanation for this performance difference is that when we add less weight, the model might ignore the positive samples because of the high similarity of both hard negative ones and positive ones. Moreover, if we apply too much weight, the model will focus too much on positive samples, ignoring the similarity caused by similar diseases among patients, resulting in the decline of performance. Therefore, we believe our setting

is a trade-off between focus and ignorance.